Talanta 105 (2013) 117–123

Contents lists available at SciVerse ScienceDirect

Talanta

journal homepage: www.elsevier.com/locate/talanta

Rapid and large-scale synthesis of pitaya-like silver nanostructures as highly efficient surface-enhanced Raman scattering substrates

Qingli Huang, Xiashi Zhu *

College of Chemistry & Chemical Engineering, Yangzhou University, Yangzhou 225009, China

ARTICLE INFO

Article history:
Received 30 August 2012
Received in revised form
22 November 2012
Accepted 25 November 2012
Available online 1 December 2012

Keywords:
Ag nanostructures
Wet-chemical methods
Surface-enhanced Raman scattering
Rhodamine 6G

ABSTRACT

A new wet-chemical approach to prepare surface-enhanced Raman scattering (SERS)-active substrates with pitaya-like silver nanostructures (PSNs) was proposed. It has been found that the morphology of as-prepared products is dependent on the reaction parameters. PSNs exhibit a high detection sensitivity of surface-enhanced Raman scattering for Rhodamine 6G (R6G) with a limit of detection of 1.0×10^{-13} mol L^{-1}. This facile, large-scale, low-cost, and green chemistry synthesized Ag nanostructures make it a perfect choice for practical SERS detection applications.

1. Introduction

The surface-enhanced Raman spectroscopy (SERS) has become a promising analytical method for rapid and accurate detection of chemicals and biochemicals since its initial discovery in 1974 [1–6]. SERS could provide a powerful means of obtaining vibrational information on adsorbate–surface interactions in view of its unique sensitivity and excellent frequency resolution from the large increase in scattering [7,8]. For its potential application, SERS-based substrates has been extensively investigated in the past decades [9,10]. To date, various SERS substrates of several materials in different shapes and structures have been reported [11–17]. Silver has been demonstrated as the most suitable material for SERS. Much attention has been focused on the size- and shape-controlled synthesis of silver nanostructures after Kneipp's group and Nie's group reported a great enhancement of Ag substrates and thereby single molecule detection by SERS [18,19]. Ag nanostructures, such as particles [20–22], rods [23,24], wires [25], plates [26–28], sheets [29], mocrospheres [30], cubes [31,32], dendritic and flower-like structures [33–44] and so forth, have been prepared by different methods.

Recently, three dimensional (3D) hierarchical metal nanostructures have been attracted much attention due to their special fine structure and large specific surface area. Both theoretical calculations and experimental measurements have showed strong enhancement of the electromagnetic field near the surface of these 3D complex structures [45–47]. Moreover, nanotextured surface structure in 3D nanoparticles can lead to significantly higher local field enhancement factors compared to those obtained with smooth particles, thus dramatically improving the Raman signals [48]. Various chemical and physical procedures have been devised to synthesize 3D Ag nanostructures with different morphologies and explore their SERS properties [33–44]. For example, Ren et al. have reported morphology-controllable synthesis of Ag dendrites in presence of PVP (polyvinylpyrrolidine) based on a facile wet-chemical route and the relation between the morphology and the SERS activity of Ag dendrites was investigated. It was shown that the smaller Ag dendrites with a lower *L*/*D* (the ratio of the length of the branches to the body diameter of the Ag dendrites) exhibited larger SERS activity [42]. The flower-like silver structures was synthesized by wet-chemical methods in the presence of PVP, which showed SERS effect of Rhodamine 6G with 10^{-6} mol L^{-1} [44]. However, the above methods normally were involved in the reduction of silver salts in the presence of potentiostat or surfactants, or at elevated temperature, or requiring the removal of template/substrate to get pure products. Therefore, developing a facile and template-free method to prepare hierarchical Ag structures is of scientific and practical importance.

In this paper, a facile wet-chemical route to the large-scale synthesis of pitaya-like silver nanostructures was demonstrated. To the best of our knowledge, the synthesis of such Ag structures has not been reported thus far. Compared to the reports referred to above, this method has two obvious advantages: (i) It is a facile and environmentally friendly method conducted at room temperature without using any seeds or sacrificial substrates; (ii) the absence in the reaction solution of potentiostat or organic surfactants provides a relatively "clean" environment to grow silver nanostructures.

* Corresponding author. Tel./fax: +86 514 7975244.
E-mail address: xszhu@yzu.edu.cn (X. Zhu).

0039-9140/$ - see front matter © 2012 Elsevier B.V. All rights reserved.
http://dx.doi.org/10.1016/j.talanta.2012.11.067

As a consequence, these relatively "clean" surfaces could be easily modified with different molecules for further applications. R6G is one of the most commonly used dye molecules to characterize the SERS enhancement of silver substrates. R6G samples of ultralow concentration were used to verify the dependence of the enhancement effect of this SERS-active substrate on their size and morphologies of Ag nanostructures.

2. Experimental

2.1. Material and apparatus

All the chemical reagents used in this work, including silver nitrate ($AgNO_3$), hydrogen peroxide (H_2O_2,Wt 30%), hydrazine hydrate ($N_2H_4 \cdot H_2O$, Wt 85%), 4-mercaptobenzoic acid (4-MBA), bovine serum albumin (BSA) and Rhodamine 6G (R6G), are analytically pure and were used as received without further purification. Deionized water was used throughout the experiment.

The phase purity of the products was characterized by X-ray diffraction (XRD, German Bruker AXSD8 ADVANCE X-ray diffractometer) using a X-ray diffractometer with Cu KR radiation (λ) 1.5418 Å). Scanning electron microscope (SEM) images were obtained using a HITACHI S-4800 microscope (Japan). Transmission electron microscope (TEM) and high resolution transmission electron microscopy (HRTEM) observations were carried out on a HRTEM FEI F-30 instrument (operated at 300 kV). Raman spectra were measured using a Britain Renishaw Invia Raman spectrometer with a solid-state laser (excitation at 532 nm, 35 mW) at room temperature in the range of 1800–800 cm^{-1}. Spectra were accumulated 3 scans, each with an exposure time of 10 s. The total accumulation time for SERS and Raman measurements was 30 s. The beam diameter was approximately 1 μm on the sample surface.

2.2. Procedures

2.2.1. Sample preparation

In a typical synthesis route, 1 mmol of $AgNO_3$ was dissolved in 20 mL of glycol at room temperature, followed by the addition of 5 drops H_2O_2. The solution was stirred at room temperature for 5 min. Then, 20 drops $N_2H_4 \cdot H_2O$ were added to the above solution. The mixture was stirred at room temperature for 0.5 h. Finally, the product was separated from the solution by centrifugation, washed several times with alcohol. The products obtained from different reaction conditions were denoted as S1–S18. A summary of the reaction conditions is listed in Table 1.

Table 1
Summary of the reaction conditions and morphologies of the products.

Sample	H_2O_2 (drops)	$N_2H_4 \cdot H_2O$ (drops)	Solvents	Morphology
S1	5	20	Glycol	Pitaya-like
S2	20	20	Glycol	Flower-like
S3	50	20	Glycol	Polyhedra
S4	0	20	Glycol	Irregular particles
S5	5	5	Glycol	Nanoparticles
S6	5	50	Glycol	Sphere-like
S7	5	20	Ethanol	Irregular particles
S8	5	20	Water	Irregular particles
S9	0	20	Ethanol	Irregular particles
S10	0	20	Water	Irregular particles
S11	5	5	Ethanol	Irregular particles
S12	5	5	Water	Flower-like
S13	5	50	Ethanol	Flower-like
S14	5	50	Water	Sphere-like
S15	20	50	Ethanol	Irregular particles
S16	20	50	Water	Irregular particles
S17	50	20	Ethanol	Polyhedra
S18	50	20	Water	Irregular blocks

2.2.2. Characterization

The as-prepared silver nanocrystals were characterized by X-ray diffraction, scanning electron microscopy, transmission electron microscopy, high resolution transmission electron microscopy and Raman spectrometer.

2.2.3. SERS

Rhodamine 6G (R6G) dye were used as Raman probe for the SERS measurements. For preparation of SERS substrates, the as-prepared Ag products were immersed in different concentration of dilute solutions of R6G for 24 h, respectively. Then these silver sample solutions were carefully dropped on specially cleaned glass slides and dried in air. Finally, the SERS of the samples were measured using a Britain Renishaw Invia Raman spectrometer with a solid-state laser (excitation at 532 nm, 35 mW) at room temperature in the range of 1800–800 cm^{-1}.

3. Results and discussion

3.1. Synthesis and characterization of silver nanostructures (PSNs)

To optimize the synthesis procedure, a series of experiments were also carried out through varying the reaction conditions such as the amount of H_2O_2, the amount of $N_2H_4 \cdot H_2O$ and the type of solvents.

3.1.1. Effect of the amount of H_2O_2 on the size and the morphology of Ag nanocrystals

It was found that H_2O_2 played an important role in determining the morphology of Ag nanocrystals. Fig. 1 is the SEM images of Ag nanocrystals prepared with different amounts of H_2O_2. Pitaya-like silver nanostructures (PSNs) were synthesized with 5 drops H_2O_2 (S1). From the SEM observations, it could be seen that (1) Ag products contain numerous pitaya-like particles with diameters about 0.5 μm (Fig. 1a), and many nanoparticles were distributed on the surface of such structure (Fig. 1b); (2) when the amount of H_2O_2 was increased to 20 drops (S2), monodispersed flower-like silver nanostructures consisting of many protuberant nanoplates were obtained (Fig. 1c and d), the average overall dimension of these Ag microflowers was 1.0 μm, and the nanoplates had a variety of shapes and sizes; (3) silver polyhedra with diameters of 1.0 μm were formed with further increasing the amount of H_2O_2 to 50 drops (S3) and the surface of the Ag products became very smooth(Fig. 1e and f); (4) only irregular particles (S4) with sizes ranging from tens of nanometers to several hundred nanometers were found in the absence of H_2O_2 (Fig. 1g and h).

3.1.2. Effect of the amount of $N_2H_4 \cdot H_2O$ on the size and the morphology of Ag nanocrystal

Fig. 2 is the SEM images of the Ag nanocrystals prepared with different amounts of $N_2H_4 \cdot H_2O$. It was evident that (1) when 5 drops $N_2H_4 \cdot H_2O$ were used (S5), only silver nanoparticles ranging from 100 to 500 nm in size were prepared (Fig. 2a); (2)when the amount of $N_2H_4 \cdot H_2O$ was increased to 20 drops (S1), pitaya-like silver nanostructures (PSNs) were synthesized as shown in Fig. 1a and b; (3)when the amount of $N_2H_4 \cdot H_2O$ was further increased to 50 drops (S6), sphere-like silver nanostructures with about 500 nm were obtained (Fig. 2b). No nanoparticles were found on the surface of sphere-like silver nanostructures (SSNs). From these results, it was revealed that the amount of $N_2H_4 \cdot H_2O$ was a major factor affecting the formation of special shapes of Ag nanocrystals.

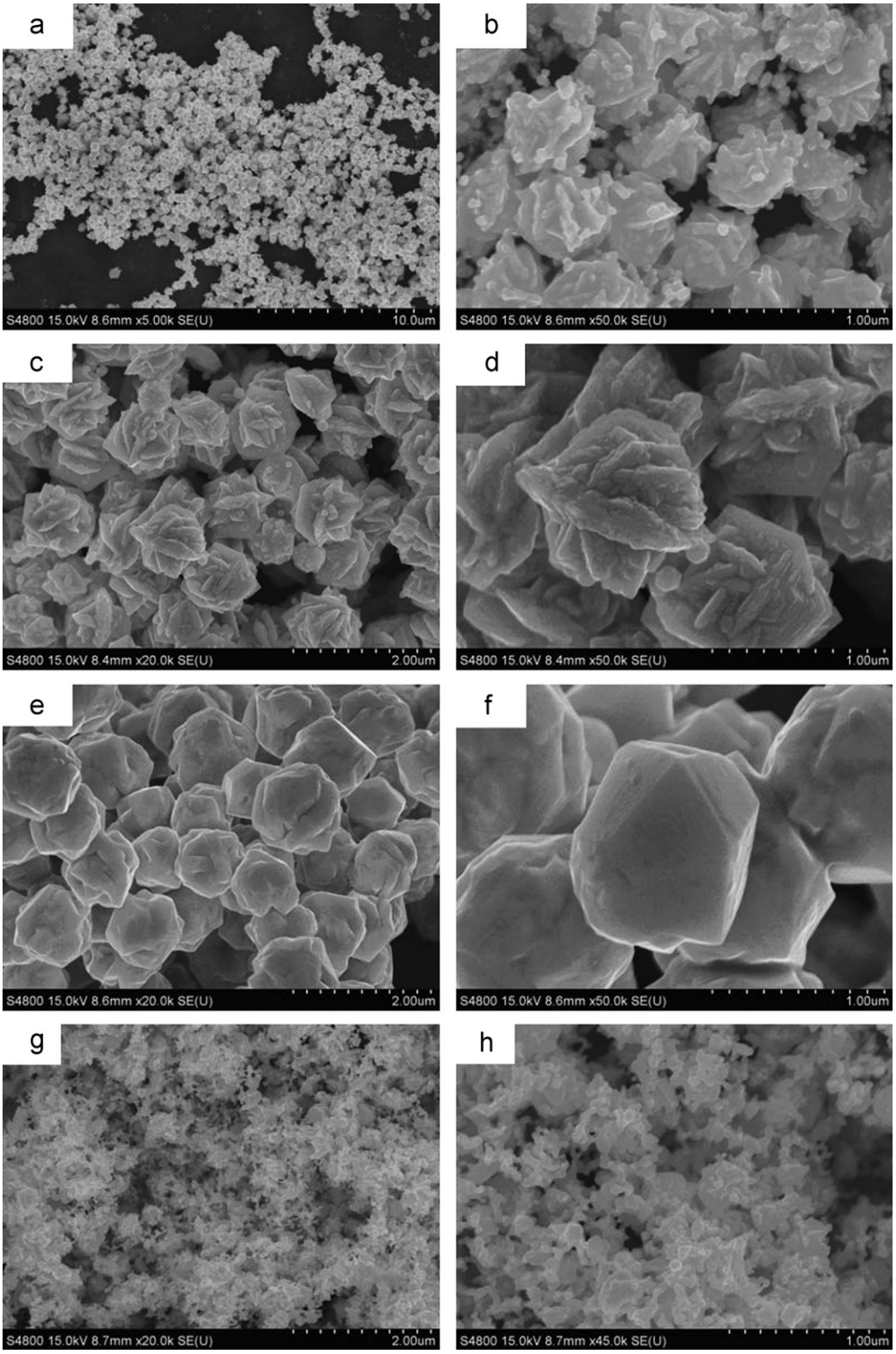

Fig. 1. SEM images of Ag nanocrystals prepared in glycol with different amounts of H_2O_2: (a–b), correspond to S1; (c–d), to S2; (e–f), to S3; (g–h), to S4.

3.1.3. Effect of solvents on the size and the morphology of Ag nanocrystals

Solvent could greatly affect the morphology and microstructure of the products [49]. The effect of the glycol, ethanol or water was investigated (Figs. 1a and b 3a and b) According to the above discussion, pitaya-like silver nanostructures (PSNs) were prepared in glycol (S1, Fig. 1a and b). However, the products had irregularly shaped morphologies with sizes ranging from 100 nm to several micrometers when ethanol was the solvent (S7, Fig. 3a) and became larger irregular blocks with several micrometers in size when water was the solvent (S8, Fig. 3b). Accumulation of particles was very distinct along with change of the polarity of solvent. Water is a dipolar, amphiprotic solvent with a high dielectric constant while ethanol has a low dielectric constant,

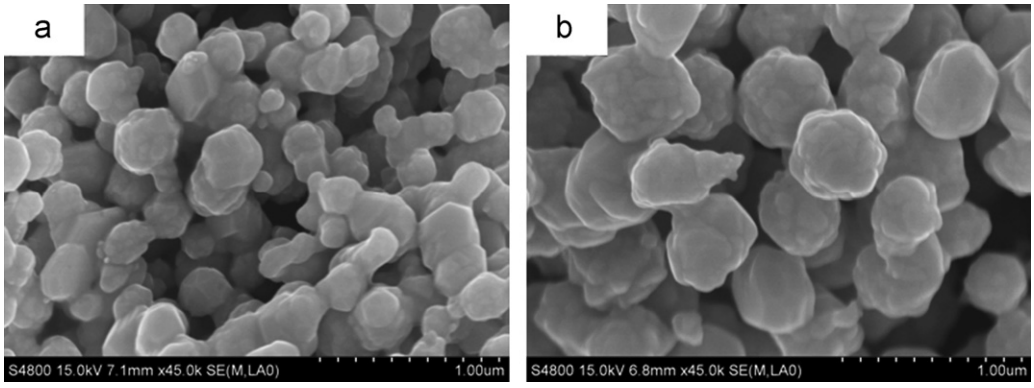

Fig. 2. SEM images of Ag nanocrystals prepared in glycol using different amounts of $N_2H_4 \cdot H_2O$: (a) S5; (b) S6.

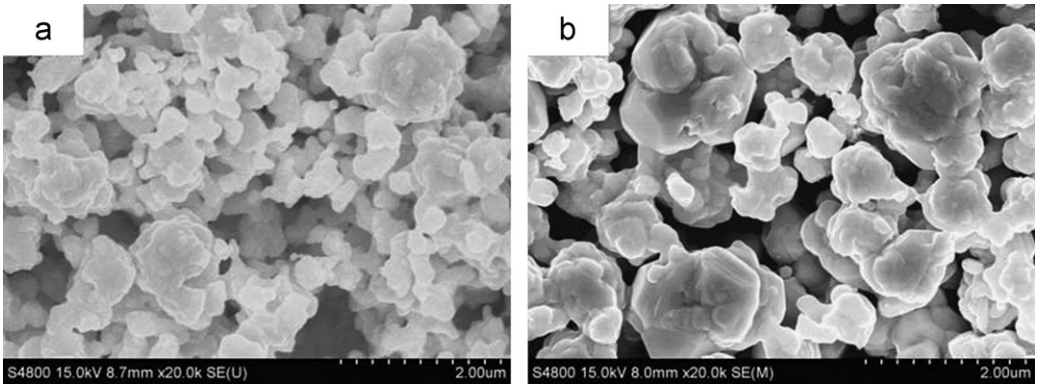

Fig. 3. SEM images of Ag nanocrystals prepared in different solvents (20 mL): (a) S7; (b) S8.

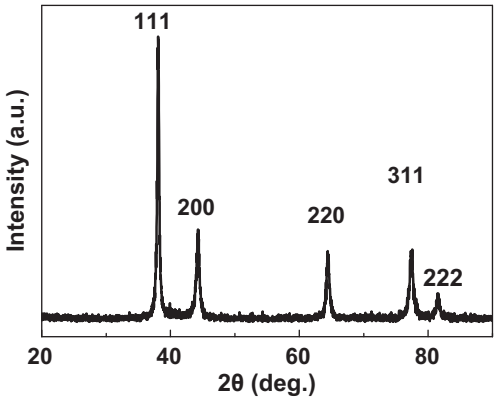

Fig. 4. XRD patterns of the as-prepared pitaya-like silver nanostructures (PSNs).

weak polarity and low surface tension. The polarity of glycol is between ethanol and water. The degree of the nonequilibrium and anisotropic growth would be different and the observed morphology would change with variation of solvent. Other experiment in ethanol and water were also carried out. The products all had various morphologies with sizes ranging from 100 nm to several micrometers as listed in Table 1 (S9–S18).

According the above detailed experiments, the optimum conditions for obtaining pitaya-like silver nanostructures (PSNs) are the following: 1 mmol $AgNO_3$, 5 drops H_2O_2, 20 drops $N_2H_4 \cdot H_2O$, and glycol solvent.

3.1.4. Characterization of pitaya-like silver nanostructures (PSNs)

XRD, TEM, and HRTEM analysis were also performed for the pitaya-like silver nanostructures; Fig. 4 displays the typical diffraction pattern of pitaya-like silver nanostructures (PSNs). The four diffraction peaks were indexed as (1 1 1), (2 0 0), (2 2 0), and (3 1 1) planes of the face centered cubic (fcc) phase silver, which was in agreement with the reported date (R=0.409 nm, JCPDS No. 4-783). No peaks of impurities were detected from this pattern. The strong and sharp peaks indicated that the as-obtained products were highly crystallized.

The TEM image in Fig. 5(a) was further confirmed by their pitaya-like hierarchical structures doped with many nanoparticles. Fig. 5(b) depicts the typical HRTEM image of an individual Ag nanoparticle. The clearly resolved lattice fringes were 0.24 nm, indicating that the Ag nanoparticles were single crystal in nature. The selected area electron diffraction of single PSN (SAED, Fig. 5c) indicated the whole structures were ploycrystine [50].

3.2. Formation mechanism of the three-dimensional (3D) pitaya-like silver nanostructures (PSNs)

On the basis of the above experimental results and corresponding analysis, a possible mechanism was proposed. It is well-known that the potentials of H_2O_2 in both acidic and alkaline solutions are higher than that of Ag^+/Ag (E°=0.7996 V); H_2O_2 can be used as an effective etchant to dissolve metallic silver. With the addition of $N_2H_4 \cdot H_2O$, there should be a subtle dynamic equilibrium between the reduction of silver particles by $N_2H_4 \cdot H_2O$ and oxidative dissolution of metallic silver by H_2O_2 in glycol. As well known, H_2O_2 could remove the relatively unstable nanoparticles, leaving only the most stable ones. When few H_2O_2 (5d and 20d) were used, nanoscale particles were maintained on the surface of the final products. However, when the sufficient H_2O_2 were used, nanoscale particles were etched by H_2O_2 and the surface of the products became smooth. The net effect of H_2O_2 in this reaction is to promote the nucleation of

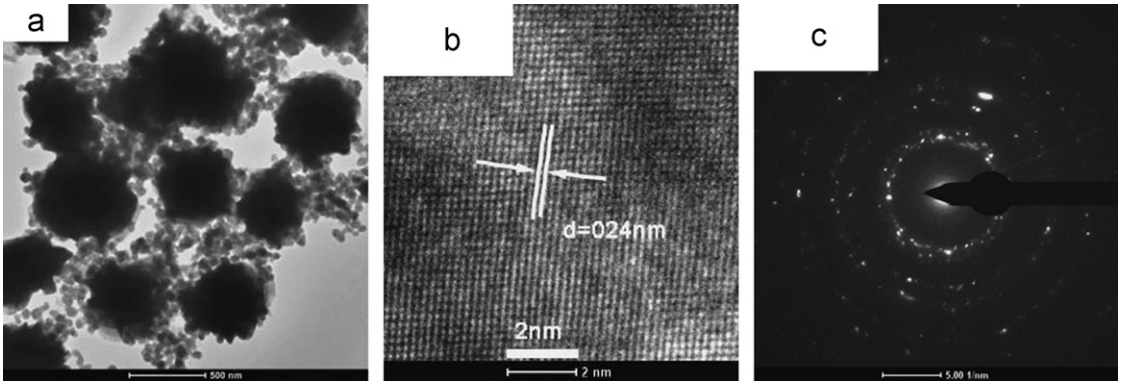

Fig. 5. Further characterization of the as-prepared pitaya-like silver nanostructures (PSNs): (a) TEM; (b) HRTEM; (c) SEAD.

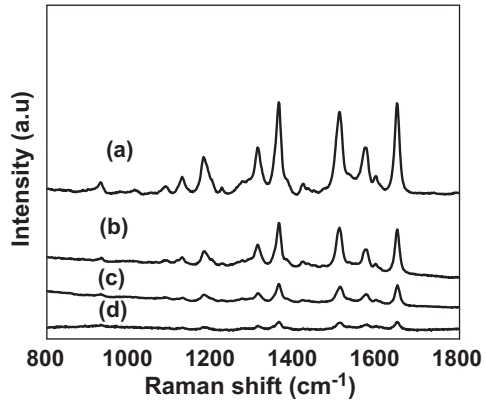

Fig. 6. SERS spectra of 10^{-6} mol L^{-1} R6G dropped on Ag nanocrystals prepared in glycol with different amounts of H_2O_2: (a) 5 drops; (b) 20 drops; (c) 50 drops; (d) 0 drop (note: the amount of $N_2H_4 \cdot H_2O$ is 20 drops).

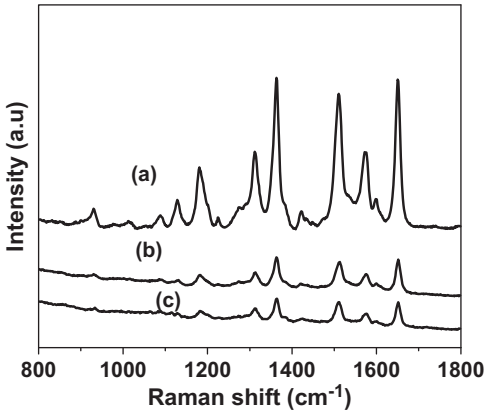

Fig. 7. SERS spectra of 10^{-6} mol L^{-1} R6G dropped on Ag nanocrystals prepared in glycol with different amounts $N_2H_4 \cdot H_2O$. (a) 20 drops; (b) 5 drops; (c) 50 drops (note: the amount of H_2O_2 is 5 drops).

monodispersed structures by removing less stable silver nanoparticles of other structures.

3.3. Effect of reaction parameters on SERS performances of R 6G

3.3.1. SERS performances of the Ag nanocrystals prepared in Section 3.1.1 (S1–S4)

Fig. 6 describes the SERS spectra of different Ag nanostructures prepared in Section 3.1.1 (S1–S4) by using R6G (1×10^{-6} mol L^{-1}) as model Raman probes. The peaks from 800 to 1800 cm^{-1} were attributed to R6G signals. The Raman peaks at 1128 (C–H bend), 1180, 1312, 1363 (aromatic C–C stretching), 1510 (aromatic C–C stretching), 1571 (aromatic C–C stretching), and 1651 cm^{-1} (aromatic C–C stretching) were characteristic vibrations of R6G [51]. The Ag three-dimensional (3D) pitaya-like silver nanostructures (S1, PSNs) displayed the strongest SERS signal intensity, which decreased with decreasing roughness (Fig. 6, curves a–c). The SERS signal intensity of Ag flower-like structures (S2) was moderate (Fig. 6, curve b). And the SERS signal intensity of Ag polyhedra (S3) was weaker, which likely due to the isolated polyhedra with smooth surface usually yielding a weak SERS response compared to complex nanostructures (Fig. 6, curve c). The SERS signal intensity of irregular Ag nanostructures (S4) prepared in absence of H_2O_2 was weakest (Fig. 6, curve d).

3.3.2. SERS performances of the Ag nanocrystals prepared in Section 3.1.2 (S5–S6)

Fig. 7 shows SERS spectra of R6G with 10^{-6} mol L^{-1} adsorbed on silver nanocrystals prepared in Section 3.1.2 (S5–S6). It was clear that the Ag nanocrystals prepared by adding 20 drops $N_2H_4 \cdot H_2O$ (S1) exhibited the highest enhancement efficiency (Fig. 7, curve a). The SERS signal intensity of silver nanoparticles (S5) was moderate (Fig. 7, curve b) and the SERS signal intensity of sphere-like silver nanostructures (S6) was weakest (Fig. 7, curve c)

3.3.3. SERS performances of the Ag nanocrystals prepared in Section 3.1.3(S7–S8)

Fig. 8 demonstrates SERS spectra of R6G (1×10^{-6} mol L^{-1}) adsorbed on Ag nanocrystals prepared in different solvents. The SERS signal intensity of pitaya-like silver nanostructures (S1, PSNs) obtained in glycol (Fig. 8, curve a) displayed better SERS performances than the other two Ag nanocrystals prepared in either ethanol (S7, Fig. 8, curve b) and water (S8, Fig. 8, curve c), respectively.

3.4. Analytical application for R6G

3.4.1. SERS of R6G with different concentrations

Encouragingly, the as-obtained pitaya-like silver nanostructures (S1, PSNs) significantly reduce the detection limit of R6G. Well-defined Raman signals of R6G are demonstrated in Fig. 9. The spectral intensities and resolutions were decreased by diluting the concentration of the target molecule (Fig. 9, curves a–j). It is found that additional R6G peaks still appeared at about 1510 and 1651 cm^{-1} (Fig. 9, curve h). Clearly, the detection concentration for R6G on the pitaya-like silver nanostructures (PSNs) substrates is as low as 10^{-13} mol L^{-1}, and thus it could be used as a "fingerprint" for the detection of R6G.

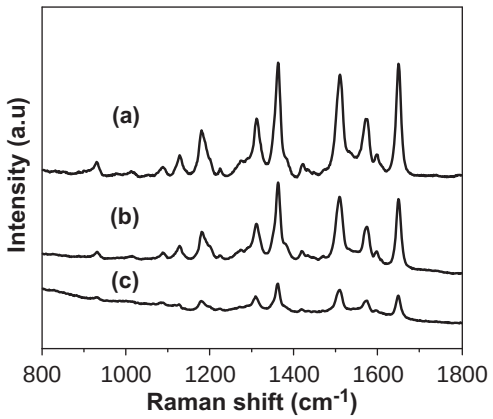

Fig. 8. SERS spectra of 10^{-6} mol L^{-1} R6G dropped on Ag nanocrystals prepared in different solvents. (a) glycol; (b) ethanol; (c) water (note: the amount of $N_2H_4 \cdot H_2O$ is 20 drops and the amount of H_2O_2 is 5 drops).

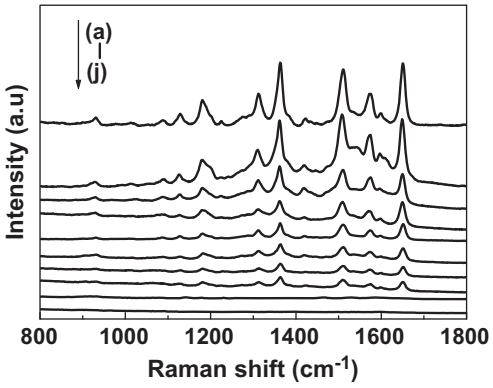

Fig. 9. SERS spectra of different concentration of R6G dropped on the as-prepared pitaya-like silver nanostructures (PSNs). (a) 10^{-6} mol L^{-1} (b) 10^{-7} mol L^{-1}; (c) 10^{-8} mol L^{-1}; (d) 10^{-9} mol L^{-1}; (e) 10^{-10} mol L^{-1}; (f) 10^{-11} mol L^{-1}; (g) 10^{-12} mol L^{-1}; (h) 10^{-13} mol L^{-1}; (i) 10^{-14} mol L^{-1}; (j) 10^{-16} mol L^{-1}.

Table 2
The linear relationship between the concentration (lg(C)) of R6G and the SERS intensity (lg(I)) at 1363 cm^{-1}.

Curve	Linear equation	Concentration(mol L^{-1})	r^2
AB	$lgI = -0.2088lgc + 6.122$	10^{-7}–10^{-9}	0.9993
BC	$lgI = -0.078lgc + 4.82$	10^{-10}–10^{-13}	0.9941

3.4.2. Analysis of characteristic of R6G

The observed Raman bands are assigned to (C–C) stretching of R6G mode at 1363 cm^{-1} [51]. Fig. 2S depicts the relationship between the R6G concentration and the intensity in a lg(I)−lg(C) style plot of the SERS signal at 1363 cm^{-1}. There are two linear relationships between the SERS intensity and the concentration of R6G over the range from 10^{-7} to 10^{-13} mol L^{-1} at 1363 cm^{-1} (Table 2).

The detection limit is as low as 10^{-13} mol L^{-1}. Such PSNs exhibit a high detection sensitivity of Rhodamine 6G (R6G) compared to early reported articles in Table 3.

3.4.3. Detection of R6G in chili pepper powers

Some chili pepper powers were mixed with R6G to improve their color. The applications of proposed method were evaluated for detection of R6G in a chili pepper powers on sale (Fig. 10). It is well known that the peak at 1651 cm^{-1} is characteristic of R6G.

Table 3
SERS performance of Rhodamine 6G (R6G) absorbed on various Ag nanostructures in early reported articles.

Methods	Morphologies	Lowest concentration of R6G (mol L^{-1})	References
Wet-chemical	Nanosheets	10^{-6}	[29]
Wet-chemical	Flower-like structures	10^{-6}	[44]
Wet-chemical	Flower-like structures	10^{-4}	[52]
Wet-chemical	Nanoparticles	10^{-9}	[53]
Wet-chemical	Pitaya-like silver nanostructures	10^{-13}	This work

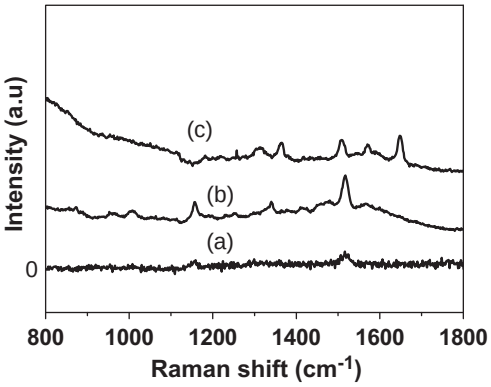

Fig. 10. SERS spectra of chili pepper powers. (a) Pure chili pepper powers; (b) pure chili pepper powers absorbed on PSNs; (c) chili pepper powers doped with 10^{-13} mol L^{-1} R6G absorbed on PSNs.

Chili pepper powers were found to be free or undetectable values from R6G (Fig. 10, curve a). The peaks at 1516, 1342, and 1158 cm^{-1} were enhanced when chili pepper powers absorbed on pitaya-like silver nanostructures (S1, PSNs), which should be Raman signals of organic compounds in chili pepper powers(Fig. 10b). However, the Raman signals of R6G were found when the sample doped with 10^{-13} mol L^{-1} R 6G (Fig. 10, curve c).

4. Conclusions

In summary, 3D pitaya-like silver nanostructures doped with nanoscale particles have been successfully prepared via a simple and green synthetic method on a large scale. The shape, size and surface fine structures of the products could be controlled well by changing the reaction parameters. The relationship between the morphologies of the products and SERS efficiency of R6G absorbed on these products were investigated. The detection limits for R6G of the optimized pitaya-like silver nanostructures approach 10^{-13} mol L^{-1}. The pitaya-like silver nanostructures could serve as better substrates for SERS applications and provide an excellent candidate for SERS analysis.

Acknowledgments

The authors acknowledge the financial support from the National Natural Science Foundation of China (20875082, 21155001), Technology Invention Foundation of Yangzhou

University (027364004015304), Invention Foundation of Jiangsu and a Project Funded by the Priority Academic Program Development of Jiangsu Higher Education Institutions and the Foundation of the Excellence Science and Technology Invention Team in Yangzhou University and the Graduate Innovation Project Foundation of Jiangsu province (CXZZ12_0894).

Appendix A. Supporting information

Supplementary data associated with this article can be found in the online version at http://dx.doi.org/10.1016/j.talanta.2012.11.067.

References

[1] M. Fleischmann, P.J. Hendra, A.J. McQuillan, Chem. Phys. Lett. 26 (1974) 163–166.
[2] A. Sengupta, N. Brar, E.J. Davis, J. Colloid Interface Sci. 309 (2007) 36–43.
[3] F. Yan, T. Vo-Dinh , Sens. Actuators B 121 (2007) 61–66.
[4] J.D. Guingab, B. Lauly, B.W. Smith, N. Omenetto, J.D. Winefordner, Talanta 74 (2007) 271–274.
[5] D. Millo, A. Bonifacio, M.R. Moncelli, V. Sergo, C. Gooijer, G. van der Zwan, Colloid Surf. B 81 (2010) 212–216.
[6] N.P.W. Pieczonka, G. Moula, R.F. Aroca, Langmuir 25 (2009) 11261–11264.
[7] Y.C. Liu, C.C. Yu, C.C. Wang, J. Mater. Chem. 17 (2007) 2120–2124.
[8] P.A. Mosier-Boss, S.H. Lieberman, Langmuir 19 (2003) 6826–6836.
[9] X.F. Liu, C.H. Sun, N.C. Linn, B. Jiang, P. Jiang, J. Phys. Chem. C 113 (2009) 14804–14811.
[10] H.Y. Liang, Z.P. Li, W.Z. Wang, Y.S. Xu, H.X. Xu, Adv. Mater. 21 (2009) 4614–4618.
[11] X.M. Lin, Y. Cui, Y.H. Xu, B. Ren, Anal. Bioanal. Chem. 394 (2009) 1729–1745.
[12] R.J.C. Brown, M.J.T. Milton, J. Raman Spectrosc. 39 (2008) 1313–1326.
[13] M.J. Banholzer, J.E. Millstone, L. Qin, C.A. Mirkin, Chem. Soc. Rev. 37 (2008) 885–897.
[14] G.W. Lu, C. Li, G.Q. Shi, Chem. Mater. 19 (2007) 3433–3440.
[15] A. Musumeci, D. Gosztola, T. Schiller, N.M. Dimitrijevic, V. Mujica, D. Martin, T. Rajh, J. Am. Chem. Soc. 131 (2009) 6040–6041.
[16] I. Alessandri, J. Colloid Interface Sci. 351 (2010) 576–579.
[17] C.W. Cheng, B. Yan, S.M. Wong, X.L. Li, W.W. Zhou, T. Yu, Z.X. Shen, H.Y. Yu, H.J. Fan, ACS Appl. Mater. Interfaces 2 (2010) 1824–1828.
[18] K. Kneipp, Y. Wang, H. Kneipp, L.T. Perelman, I. Itzkan, R. Dasari, M.S. Feld, Phys. Rev. Lett. 78 (1997) 1667–1670.
[19] S.M. Nie, S.R. Emery, Science 275 (1997) 1102–1106.
[20] A. Pal, S. Shah, S. Devi, Mater. Chem. Phys. 114 (2009) 530–532.
[21] R.M. Liu, M.Z. Si, Y.P. Kang, X.F. Zi, Z.Q. Liu, D.Q. Zhang, J. Colloid Interface Sci. 343 (2010) 52–57.
[22] G. Paul, S. Sarkar, T. Pal, P.K. Das, I. Manna, J. Colloid Interface Sci. 371 (2012) 20–27.
[23] M.R. Hormozi-Nezhada, M. Jalali-Heravi, H. Robatjazia, H. Ebrahimi- Najafabadia, Colloids Surf. A: Physicochem. Eng. Aspects 393 (2012) 46–52.
[24] J. Zhang, M.R. Langille, C.A. Mirkin, Nano Lett. 11 (2011) 2495–2498.
[25] T. Tetsumoto, Y. Gotoh, T. Ishiwatari, J. Colloid Interface Sci. 362 (2011) 267–273.
[26] T.C.R. Rocha, D. Zanchet, J. Phys. Chem. C 111 (2007) 6989–6993.
[27] B.H. Lee, M.S. Hsu, Y.C. Hsu, C.W. Lo, C.L. Huang, J. Phys. Chem. C 114 (2010) 6222–6227.
[28] G.L. Si, W.T. Shi, K. Li, Z.F. Ma, Colloids Surf. A: Physicochem. Eng. Aspects 380 (2011) 257–260.
[29] H.J. Chen, F. Simon, A. Eychmuller, J. Phys. Chem. C 114 (2010) 4495–4501.
[30] T. Preuksarattanawut, S. Asavavisithchai, E. Nisaratanaporn, Mater. Chem. Phys. 130 (2011) 481–486.
[31] S.E. Skrabalak, L. Au, X.D. Li, Y.N. Xia, Nat. Protocols 2 (2007) 2182–2190.
[32] A.R. Siekkinen, J.M. McLellan, J.Y. Chen, Y.N. Xia, Chem. Phys. Lett. 432 (2006) 491–496.
[33] Y.L. Wei, Y.S. Chen, L.J. Ye, P.M. Chang, Mater. Res. Bull. 46 (2011) 929–936.
[34] A. Gute, C. Carraro, R. Maboudian, J. Am. Chem. Soc. 132 (2010) 1476–1477.
[35] Y.Y. Xia, J.M. Wang, Mater. Chem. Phys. 125 (2011) 267–270.
[36] W.M. Cheng, C.C. Wang, C.Y. Chen, J. Colloid Interface Sci. 348 (2010) 49–56.
[37] Q. Zhou, S. Wang, N. Jia, L. Liu, J. Yang, Z. Jiang, Mater. Lett. 60 (2006) 3789–3792.
[38] S.C. Tang, X.K. Meng, H.B. Lu, S.P. Zhu, Mater. Chem. Phys. 116 (2009) 464–468.
[39] L. Fan, R. Guo, Cryst. Growth Des. 8 (2008) 2150–2156.
[40] Y.L. Wang, P.H.C. Camargo, S.E. Skrabalak, H.C. Gu, Y.N. Xia, Langmuir 24 (2008) 12042–12046.
[41] G.X. Zhang, S.H. Sun, M.N. Banis, R.Y. Li, M. Cai, X.L. Sun, Cryst. Growth Des. 11 (2011) 2493–2499.
[42] W. Ren, S.J. Guo, S.J. Dong, E.K. Wang, J. Phys. Chem. C 115 (2011) 10315–10320.
[43] Z. Zheng, S.C. Tang, S. Vongehr, X.K. Meng, Chem. Phys. 129 (2011) 594–598.
[44] T. Liu, D.S. Li, D.R. Yang, M.H. Jiang, Langmuir 27 (2011) 6211–6217.
[45] J.F. Li, Y.F. Huang, Y. Ding, Z.L. Yang, Nature 464 (2010) 392–395.
[46] H. Wang, N.J. Halas, Adv. Mater. 20 (2008) 820–825.
[47] P.S. Kumar, I. Pastoriza-Santos, B. Rodriguez-Gonzalez, F.J. Garcia de Abajo, L.M. Liz-Marzan, Nanotechnology 19 (2008) 156–160.
[48] M.F. Zhang, A.W. Zhao, H.H. Sun, H.Y. Guo, D.P. Wang, D. Li, Z.B. Gan, J. Mater. Chem. 21 (2011) 18817–18824.
[49] Y. Li, Y.Q. Guo, R.Q. Tan, P. Cui, Y. Li, W.J. Song, Mater. Lett. 63 (2009) 2085–2088.
[50] J.W. Lau, R.D. McMichael, M.J. Donahue, J. Res. Natl. Inst. Stan. 114 (2009) 57–67.
[51] P. Hildebrandt, M. Stockburger, J. Phys. Chem. 88 (1984) 5935–5944.
[52] J.H. Yang, R.C. Dennis, D.K. Sardar, Mater. Res. Bull. 46 (2011) 1080–1084.
[53] W.B. Li, Y.Y. Guo, P. Zhang, J. Phys. Chem. C 114 (2010) 6413–6417.